



Universiteit  
Leiden  
The Netherlands

## **Boron tunneling in the "weak" bond-stretch isomerization of N-B Lewis adducts**

Nandi, A.; Tarannam, N.; Silva, D.R.; Fonseca Guerra, C.; Hamlin, T.A.; Kozuch, S.

### **Citation**

Nandi, A., Tarannam, N., Silva, D. R., Fonseca Guerra, C., Hamlin, T. A., & Kozuch, S. (2021). Boron tunneling in the "weak" bond-stretch isomerization of N-B Lewis adducts. *Chemphyschem*, 22(18), 1857-1862. doi:10.1002/cphc.202100505

Version: Publisher's Version

License: [Leiden University Non-exclusive license](#)

Downloaded from: <https://hdl.handle.net/1887/3248547>

**Note:** To cite this publication please use the final published version (if applicable).

# Boron Tunneling in the “Weak” Bond-Stretch Isomerization of N–B Lewis Adducts

Ashim Nandi<sup>+</sup>,<sup>[a]</sup> Naziha Tarannam<sup>+</sup>,<sup>[a]</sup> Daniela Rodrigues Silva,<sup>[b, c]</sup> Célia Fonseca Guerra,<sup>[b, d]</sup> Trevor A. Hamlin,<sup>\*[b]</sup> and Sebastian Kozuch<sup>\*[a]</sup>

Some nitrile-boron halide adducts exhibit a double-well potential energy surface with two distinct minima: a “long bond” geometry (LB, a van der Waals interaction mostly based on electrostatics, but including a residual charge transfer component) and a “short bond” structure (SB, a covalent dative bond). This behavior can be considered as a “weak” form of bond stretch isomerism. Our computations reveal that complexes RCN–BX<sub>3</sub> (R = CH<sub>3</sub>, FCH<sub>2</sub>, BrCH<sub>2</sub>, and X = Cl, Br) exhibit a

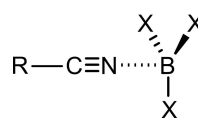
fast interconversion from LB to SB geometries even close to the absolute zero thanks to a *boron atom tunneling mechanism*. The computed half-lives of the meta-stable LB compounds vary between minutes to nanoseconds at cryogenic conditions. Accordingly, we predict that the long bond structures are practically impossible to isolate or characterize, which agrees with previous matrix-isolation experiments.

## 1. Introduction

Bond-stretch isomerism (BSI), a term coined by Stohrer and Hoffmann in the early 1970s, postulates the existence of two molecular isomeric forms differing only in a specific bond length; this is, in principle, caused by distinct electronic configurations between both structures.<sup>[1,2]</sup> While several experimental and theoretical studies invoked this concept to describe isomeric metal oxo complexes differing only in their M=O bond lengths,<sup>[3–8]</sup> these studies were criticized claiming an incorrect structural characterization.<sup>[9–12]</sup> To date, most studies on BSI revolve around theoretical models and few experimental cases are known.<sup>[13–18]</sup>

Donor-acceptor nitrile-boron RCN–BX<sub>3</sub> complexes (R = alkyl or substituted alkyl group, X = halides, see scheme 1), offer a class of species where a “weak” form of BSI can occur. The chemistry of such complexes span many decades,<sup>[19–26]</sup> and their structural and bonding properties are still an area of extensive research both for experimentalists and theoreticians.<sup>[27]</sup> The assignment of the bonding patterns in these complexes has been challenging, generally viewed as comprising electrostatic,

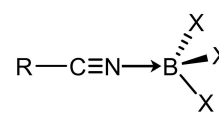
Long Bond (“LB”)



R = CH<sub>3</sub>; X = F, Cl or Br

R = FCH<sub>2</sub>, ClCH<sub>2</sub>; X = Cl

Short Bond (“SB”)



**Scheme 1.** Non-covalent long-bond (LB) and covalent dative short-bond (SB) RCN–BX<sub>3</sub> complexes, with the R and X substituent pairs studied herein.

covalent, dative, and/or charge-transfer interactions. All this depends on the nature and length of the bond,<sup>[28]</sup> blurring the distinction between covalent and non-covalent interactions. Moreover, sometimes both covalent and non-covalent possibilities arise on the same species (scheme 1). Such an unusual bonding situation was predicted in the adducts of BCl<sub>3</sub> with MeCN, FCH<sub>2</sub>CN, and ClCH<sub>2</sub>CN, characterized by two distinct minima separated by a low but significant barrier. In these, the N–B interacting distance varies between those of van der Waals and covalent interactions.<sup>[29,30]</sup>

Previous computations<sup>[29,30]</sup> showed that the double-well potentials of this class tend to have:

- 1) A long bond (“LB”) meta-stable non-covalent interaction, with an N–B bond length of ~2.6–2.9 Å.
- 2) A short bond (“SB”) global minimum dative covalent interaction, with an N–B distance of ~1.6 Å.

The barriers between these two minima lie between 4 to 11 kJ mol<sup>–1</sup> with respect to the meta-stable LB, and their corresponding reaction energies are in the range of 5–20 kJ mol<sup>–1</sup>.<sup>[29,30]</sup> This would, in principle, make it possible to observe both geometries if a high-temperature mixture of the two configurations is fast-cooled to cryogenic conditions, keep-

[a] A. Nandi,<sup>+</sup> N. Tarannam,<sup>+</sup> Prof. S. Kozuch  
Department of Chemistry, Ben-Gurion University of the Negev, Beer-Sheva 841051, Israel  
E-mail: kozuch@bgu.ac.il

[b] D. Rodrigues Silva, Prof. Dr. C. Fonseca Guerra, Dr. T. A. Hamlin  
Department of Theoretical Chemistry, Amsterdam Institute of Molecular and Life Sciences (AIMMS), Amsterdam Center for Multiscale Modeling (ACMM), Vrije Universiteit Amsterdam, De Boelelaan 1083, 1081 HV Amsterdam, The Netherlands  
E-mail: t.a.hamlin@vu.nl

[c] D. Rodrigues Silva  
Departamento de Química, Instituto de Ciências Naturais, Universidade Federal de Lavras, 37200-900, Lavras-MG, Brazil

[d] Prof. Dr. C. Fonseca Guerra  
Leiden Institute of Chemistry, Gorlaeus Laboratories, Leiden University, Einsteinweg 55, 2333 CC Leiden, The Netherlands

[\*] Equal contribution from both authors.

Supporting information for this article is available on the WWW under <https://doi.org/10.1002/cphc.202100505>

ing the system in the out-of-equilibrium original state by its kinetic barrier. However, in stark contrast with this assumption, matrix-isolation IR spectra revealed only the presence of the short-bond structure with the authors speculating that the elusive long-bond form might be masked by HCl impurities forming H-bonded adducts.<sup>[29,30]</sup>

In this work, we propose that the reason for the unsuccessful attempts of capturing and detecting the LB structure even close to the absolute zero can be attributed to heavy-atom quantum mechanical tunneling (QMT). QMT is a well-known effect for hydrogen-based reactions, but only recently it was established that “heavy” atom tunneling (i.e. second-row atoms) can also play an important role for reactions with low and, most importantly, narrow barriers.<sup>[31–36]</sup> The LB to SB reactions presented here indeed involve low barriers with relatively short trajectories. However, they also require the movement of heavy atoms, potentially hindering any realistic QMT mechanism. While experimentally testing QMT is theoretically doable by kinetic isotope effect (KIE) analysis, this would be almost impossible since no isotopic substitution would make the LB form stable enough. Therefore, only accurate computations can support the current hypothesis and validate our prediction.

### 1.1. Theoretical Method

All geometries, electronic energies, and their derivatives were computed at the M06-2X level in *Gaussian 16*.<sup>[37]</sup> This functional was found to be suitable in geometry and frequency predictions against experimental gas-phase structures of these complexes and provided good agreement with accurate post-Hartree-Fock methods.<sup>[30]</sup> Since direct dynamic tunneling computations are time-demanding, a small but optimal basis set was sought. We found that M06-2X/6-311+G(d) meets the requirements, providing a close agreement with structural parameters; the diffuse functions were included to improve the accuracy of charge transfer interactions.<sup>[27,29,30,38]</sup>

Classical (i.e. non-QMT) reaction rates were computed using canonical variational transition state theory (CVT),<sup>[39]</sup> with QMT contributions added with the small curvature tunneling (SCT)<sup>[40,41]</sup> method; a step size of 0.001 Bohr and quantized reactant state tunneling (QRST) for the reaction coordinate mode were used.<sup>[42]</sup> The M06-2X/6-311+G(d) electronic energies were corrected with a double layer method (the interpolated single-point energy -ISPE<sup>[43]</sup>), where the energies of reactants, products, and transition states were recomputed at the CCSD(T)/CBS level (obtained from aug-cc-pVTZ and aug-cc-pVQZ extrapolation with  $\beta$  coefficients of 5 and 3 for the HF and post-HF correlation, except for Br where an aug-cc-pvTZ-PP and aug-cc-pvQZ-PP basis set was employed). This double layer method can only work when the underlying DFT surface is geometrically correct,<sup>[44–46]</sup> and the *ab initio* methods are of high quality; there is no reason to suspect that these two conditions are not fulfilled in these closed shell systems.<sup>[38]</sup> Polyrate 17 was used to compute all the rate constants,<sup>[47]</sup> with Gaussrate<sup>[48]</sup> as the interface between Polyrate and Gaussian. Noteworthy, while

we consider our results reasonably accurate for gas phase, most experiments are carried out in cryogenic matrices, where there is a small but significant interaction between the solute and the matrix (typically frozen noble gases). These interactions produce anisotropic pressures, which tend to unsystematically accelerate the rates<sup>[49]</sup> (or even occasionally favoring the smaller SB in a thermodynamic way in some matrix environments) and deviate from gas phase predictions. Therefore, we consider the presented rate constants as semiquantitative, although the conclusions are still reliable even considering the medium difference.

All the binding (BE), threshold ( $\Delta E^\ddagger$ ) and reaction ( $\Delta E_r$ ) energies discussed here are CCSD(T)/CBS electronic energies plus zero-point energies at the M06-2X/6-311+G(d) level. BEs are taken with the individual monomer energies as reference.

The activation strain model (ASM)<sup>[50–55]</sup> was used to characterize the bonding mechanism in MeCN–BCl<sub>3</sub> and MeCN–BBr<sub>3</sub>. In the ASM, the electronic binding energy is divided into two major components: strain energy ( $\Delta E_{\text{strain}}$ ) that results from the distortion of the monomers (i.e. MeCN and BX<sub>3</sub>) from their equilibrium structure to the geometry they acquire in the MeCN–BX<sub>3</sub> adduct, and the actual interaction energy ( $\Delta E_{\text{int}}$ ) between the deformed monomers.  $\Delta E_{\text{int}}$  is further decomposed using the matching canonical energy decomposition analysis (EDA)<sup>[56–58]</sup> into three physically meaningful energy terms, namely, the classical electrostatic interaction ( $\Delta V_{\text{elstat}}$ ), the steric Pauli repulsion between closed-shell orbitals ( $\Delta E_{\text{Pauli}}$ ), and the stabilizing orbital interactions that account for donor-acceptor interactions and polarization ( $\Delta E_{\text{oi}}$ ). The analysis started from the optimized MeCN and BX<sub>3</sub> at a relatively large distance ( $r_{\text{B-N}} = 3.5 \text{ \AA}$ ). The fragments were then brought together by decreasing the B–N bond to a distance shorter than in their global energy minimum ( $r_{\text{B-N}} = 1.0 \text{ \AA}$ ). All energy terms are projected onto  $\xi$ , the critical reaction coordinate, which allows for the evaluation of how each energy component varies as a function of the formation of the Lewis pairs. The adducts are compared at the same point along this potential energy surface, the so-called “consistent geometry”, to ensure that our conclusions are not skewed by the fact the Lewis pairs have different equilibrium bond lengths. The calculations were performed using ZORA-M06-2X/TZ2P<sup>[59–62]</sup> as implemented in the Amsterdam Density Functional (ADF) software.<sup>[63–65]</sup> The open-source PyFrag 2019 program was used to expedite all ASM and EDA analyses.<sup>[66–68]</sup> Additionally, Natural Bond Orbital (NBO)<sup>[69,70]</sup> analyses were performed with NBO7 at the M06-2X/6-311+G(d) level in MeCN–BX<sub>3</sub> (X = H, F, Cl, Br, see SI).

## 2. Results and Discussion

### 2.1. Electronic Structure of the Donor-Acceptor Adducts

In contrast to most of the other systems considered, MeCN–BF<sub>3</sub> shows a single minimum with a N–B bond distance of 1.77 Å (too long for a covalent bond, too short for a van der Waals interaction), and a BE of  $-28.2 \text{ kJ mol}^{-1}$  (see Table 1). This suggests that the system approaches a double-well profile but

**Table 1.** RCN–BX<sub>3</sub> N–B bond distance for long-bond (LB), short bond (SB), and transition state (TS) structures in Å, and their respective binding energies (BE) along with threshold energies (from LB to TS,  $\Delta E^\ddagger$ ) and reaction energies ( $\Delta E_r$ ) in kJ mol<sup>-1</sup>, and transition state imaginary frequencies ( $\nu$ ) in cm<sup>-1</sup>.

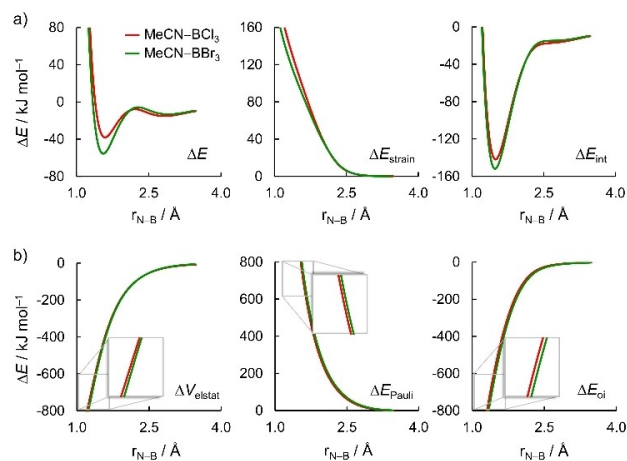
R	X	LB	SB	TS	BE <sub>LB</sub>	BE <sub>SB</sub>	$\Delta E^\ddagger$	$\Delta E_r$	$\nu$
Me	F	–	1.77	–	–	–28.2	–	–	–
Me	Cl	2.77	1.60	2.24	–13.0	–34.3	3.3	–21.2	201 <i>i</i>
Me	Br	2.89	1.57	2.29	–16.6	–51.1	3.5	–34.5	216 <i>i</i>
FCH <sub>2</sub>	Cl	2.84	1.62	2.15	–11.0	–15.9	9.0	–4.9	210 <i>i</i>
ClCH <sub>2</sub>	Cl	2.83	1.61	2.16	–11.6	–20.4	7.7	–8.8	209 <i>i</i>

actually results in a flat, barrierless potential. This is due to the fact that the B–F bond is the strongest along the series of boron trihalides and, therefore, it is more energetically costly to deform BF<sub>3</sub> to the pyramidal geometry adopted in the SB complex. As a result, it leads to a longer B–N equilibrium bond length<sup>[70]</sup> (in line with previous reports, where an extremely flat potential with two almost isoenergetic minima has been predicted for this species<sup>[27,71,72]</sup>).

MeCN–BCl<sub>3</sub> exhibits the above described double-well surface with an N–B distance of 2.77 Å for the LB, and 1.60 Å for the SB, in good agreement with previous computational results.<sup>[29]</sup> The binding energies of the LB and SB structures are –13.0 kJ mol<sup>-1</sup> and –34.3 kJ mol<sup>-1</sup>, respectively; this shows the typical (but not obligatory) trend of a stronger covalent bond compared to the van der Waals interaction. MeCN–BBr<sub>3</sub> has a slightly longer LB and shorter SB than MeCN–BCl<sub>3</sub>, with deeper wells (especially for SB, compare rows two and three in Table 1).

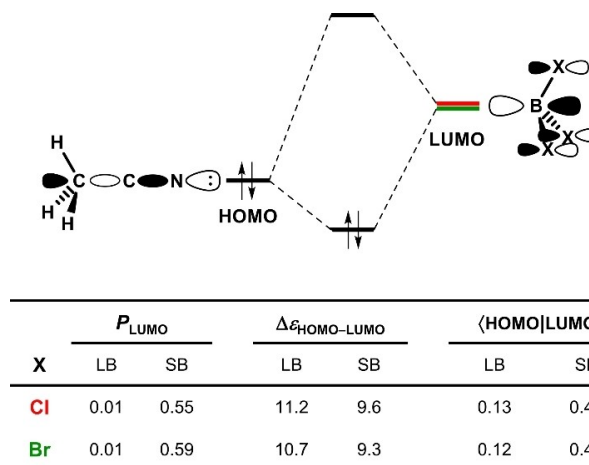
In the case of haloacetonitrile–BCl<sub>3</sub> complexes (R = FCH<sub>2</sub> or ClCH<sub>2</sub>), the N–B bond distances are almost invariant to one another (entries 4 and 5 in Table 1) and slightly longer than in the parent MeCN–BCl<sub>3</sub>. However, their binding energies are significantly weaker in comparison to the parent complex for LB but especially for SB. While the concept of charge transfer is typically used in van der Waals interactions, let us remember that a dative covalent bond can be considered as an extreme case of charge transfer (see below). The BSI of these systems is, therefore, less exergonic than in the acetonitrile complex, producing a higher threshold energy, in accordance with Hammond's principle.<sup>[73]</sup>

Next, to characterize the nature of the LB and SB complexes in the MeCN–BX<sub>3</sub> Lewis donor-acceptor adducts (X = Cl, Br, see Figure 1) we employed the activation strain model (ASM)<sup>[50–55]</sup> in combination with the matching energy decomposition analysis (EDA).<sup>[56–58]</sup> Figure 1a left nicely shows the formation of the LB and SB minima separated by a low barrier (see Table 1 and S1). The stronger BE of SB compared to LB complexes arises from an increasingly stabilizing interaction energy  $\Delta E_{\text{int}}$  (Figure 1a right) between MeCN and BX<sub>3</sub> as the N–B separation decreases. Our results demonstrate that the trend in  $\Delta E_{\text{int}}$  stems mostly from the orbital interactions  $\Delta E_{\text{oi}}$ , as observed by the steepest decrease in the  $\Delta E_{\text{oi}}$  curve in Figure 1b right. Note that for LBs the orbital interactions  $\Delta E_{\text{oi}}$  are less stabilizing than the electrostatic interactions  $\Delta V_{\text{elstat}}$  (e.g. for X = Br,  $\Delta E_{\text{oi}}$  and  $\Delta V_{\text{elstat}}$  amount to –10.5 and –21.6 kJ mol<sup>-1</sup>, respectively). This picture, however, is gradually reversed as the N–B separation decreases and the amount of charge transfer increases. For SBs, the contribution from the  $\Delta E_{\text{oi}}$  is larger than that of the  $\Delta V_{\text{elstat}}$  (e.g.

**Figure 1.** a) Activation strain model (ASM) and b) energy decomposition analysis (EDA) of the MeCN–BX<sub>3</sub> adducts (X = Cl, Br) as a function of the N–B bond distance, computed at ZORA-M06-2X/TZ2P.

for X = Br,  $\Delta E_{\text{oi}}$  and  $\Delta V_{\text{elstat}}$  are, respectively, –512.4 and –437.6 kJ mol<sup>-1</sup>), see Table S2 for data at consistent geometries.

The trends in  $\Delta E_{\text{oi}}$  can be rationalized in terms of the well-known HOMO(base)–LUMO(acid) interaction (see Figure 2). Note that the gross population ( $P_{\text{LUMO}}$ ) of the BX<sub>3</sub> LUMO

**Figure 2.** Schematic representation of the HOMO–LUMO interaction in the MeCN–BX<sub>3</sub> along with gross population of the LUMO of BX<sub>3</sub> (in electrons), orbital energy gap (in eV), and orbital overlap. Data at consistent geometries with N–B distance as in the equilibrium geometries of the MeCN–BBr<sub>3</sub> adduct. HOMO and LUMO of the a<sub>1</sub> irreducible representation of the C<sub>3v</sub> symmetry.

increases considerably from LB to SB (going from 0.01 to 0.55 and 0.59 electrons for X = Cl and Br, respectively), which can be attributed to the larger charge-transfer observed for SB. The  $\Delta E_{\text{oi}}$  energy is more stabilizing at shorter N–B distances because the  $\langle \text{HOMO} | \text{LUMO} \rangle$  orbital overlap is larger, and the  $\Delta \epsilon_{\text{HOMO-LUMO}}$  energy gap is smaller (see Figure 2 and S1). For example, for X = Br, note that  $\langle \text{HOMO} | \text{LUMO} \rangle$  increases by 0.32 (from 0.12 to 0.44) and  $\Delta \epsilon_{\text{HOMO-LUMO}}$  decreases by 1.4 eV (from 10.7 to 9.3 eV) going from LB to SB. The latter is due to the fact that the LUMO drops in energy as  $\text{BX}_3$  deforms from the planar to the pyramidal geometry (i.e. when going from an  $\text{sp}^2$  to an almost  $\text{sp}^3$  rehybridization on the boron).<sup>[74,75]</sup> Noteworthy, the NBO perturbational analysis on these  $\text{MeCN-BX}_3$  systems supports the ASM and EDA results concerning the orbital interactions (see the detailed NBO discussion in the SI).

In the SB systems, the strength of the N–B bond also significantly depends on the strain energy  $\Delta E_{\text{strain}}$  (see Figure 1a middle and the fourth entry in Table S2). As demonstrated in our previous work,<sup>[74]</sup> the N–B bond is stronger in the Lewis adducts involving boron trihalides that can more easily pyramidalize from its planar equilibrium geometry. The results shown in Figure 1a are in line with this rationalization. The B–Br bond is weaker than the B–Cl bond and, therefore, it requires less energy to deform  $\text{BBr}_3$  than  $\text{BCl}_3$ , resulting in a more stabilizing adduct with the former.<sup>[74–76]</sup> For the LB complexes,  $\Delta E_{\text{strain}}$  is nearly zero and does not contribute to the trend in  $\Delta E$ .

## 2.2. Analysis of Tunneling Rates

Considering the low threshold energies and the high exergonicity of our reactions, which in accord with Hammond's rule results in narrower barriers,<sup>[73]</sup> we ventured on the study of their tunneling reaction rates. Our computed classical (CVT) rate constants show that the LB to SB reaction for  $\text{MeCN-BCl}_3$  would be impossible at 4 K ( $k_{\text{CVT}}^4\text{K} = 4 \times 10^{-35} \text{ s}^{-1}$ , entry 2 in Table 2), and it is still negligible below 10 K ( $k_{\text{CVT}}^{10\text{K}} = 1 \times 10^{-7} \text{ s}^{-1}$ ). However, when adding the tunneling correction the reaction shows an enormous acceleration, giving a fixed rate constant of  $2 \times 10^7 \text{ s}^{-1}$  below 10 K; this indicates that the reaction is completely driven by QMT from the ground-state vibrational level at these temperatures. The Arrhenius plot in Figure 3 reveals a sharp curvature when moving to the “deep-tunneling”, temperature-independent rates (solid red line), which departs from the classical values (dotted red line) below the ~50 K region. The longest possible half-life ( $t_{1/2}$ ) for the LB geometry of  $\text{MeCN-BCl}_3$

**Table 2.** Computed rate constants without ( $k_{\text{CVT}}$ ) and with tunneling ( $k_{\text{SCT}}$ ) for  $\text{RCN-BX}_3$  in  $\text{s}^{-1}$ , and half-lives ( $t_{1/2}$ ) in seconds for the LB to SB reactions at 4 K.

R	X	$k_{\text{CVT}}$	$k_{\text{SCT}}$	$t_{1/2}$
Me	F	–	–	–
Me	Cl	$4 \times 10^{-35}$	$2 \times 10^7$	$4 \times 10^{-8}$
Me	Br	$2 \times 10^{-39}$	$1 \times 10^7$	$6 \times 10^{-8}$
FCH <sub>2</sub>	Cl	$3 \times 10^{-107}$	$5 \times 10^{-3}$	100
CICH <sub>2</sub>	Cl	$2 \times 10^{-88}$	0.8	0.8

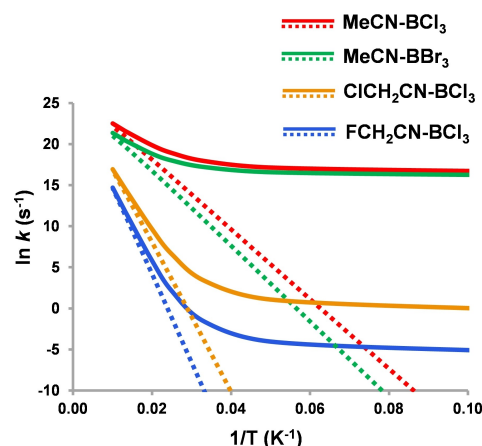


**Figure 3.** Arrhenius plot for the rate constants without (CVT, dotted lines) and with tunneling corrections (SCT, solid lines) for all the systems studied in this work.

is 40 ns, showing that LB will probably be impossible to observe experimentally, no matter how low we go in the temperature scale. This “quantum tunneling instability” (QTI)<sup>[49,77,78]</sup> can easily explain the failure to detect the theoretically predicted LB structure in cryogenic matrix isolation IR experiments.<sup>[29]</sup>

In the brominated  $\text{MeCN-BBr}_3$  adduct (entry 3 in Table 2), with a  $0.2 \text{ kJ mol}^{-1}$  higher barrier than  $\text{MeCN-BCl}_3$ , we see a similar curved Arrhenius graph (green line in Figure 3) with  $k_{\text{SCT}}^4\text{K} = 1 \times 10^7 \text{ s}^{-1}$ , corresponding to a  $t_{1/2}$  of 60 ns at 4 K. Since there are no reported experimental studies on this system, we can predict that similar to the chlorinated system, even if this complex is attempted to be synthesized and characterized, it would be impossible to capture and detect the LB form due to heavy-atom QMT.

For the monosubstituted  $\text{FCH}_2\text{CN-BCl}_3$  and  $\text{ClCH}_2\text{CN-BCl}_3$  (4<sup>th</sup> and 5<sup>th</sup> entries in Table 2), it was reported that the IR studies of these systems in nitrogen and/or neon matrices matched only the short-bonded complex.<sup>[29]</sup> Classical CVT rates show that the BSI reaction of the fluorinated case would be negligible below 30 K (see Figure 3). However, including tunneling the reaction is feasible even close to absolute zero, with  $t_{1/2}$  of circa 2 minutes at 4 K and 4 seconds at 30 K, possibly too short to be detected (unless carrying out a fast IR spectra immediately after deposition of the complex).<sup>[30]</sup> Similar conclusions were also reached for  $\text{ClCH}_2\text{CN-BCl}_3$ , with a maximum  $t_{1/2}$  of 1 s. In all these cases we predict that the difficulties to observe the non-covalently bonded LB systems can be attributed to quantum tunneling instabilities.<sup>[49,77,78]</sup>

## 2.3. Kinetic Isotope Effect

To understand which atom contributes the most to the tunneling process, we carried out a kinetic isotope effect (KIE) analysis on  $\text{MeCN-BCl}_3$ . As the tunneling probability typically depends on the collective motion of all the atoms involved in the reaction, we looked at their displacement vectors in the

transition state to identify the atoms with the wider movement in that region.<sup>[34,79,80]</sup> In principle there should be a correlation between the magnitude of these vectors and the KIE, and indeed we see a correlation between these magnitudes in Figure 4. The highest KIE and the most significant vector reside in the boron, and therefore in the N–B bond-stretch we can safely say that this is the “tunneling-determining atom”, in a rare case of boron-atom tunneling.<sup>[79]</sup>

Note that to keep the symmetry we studied the KIEs substituting all the equivalent atoms together (i.e. the three hydrogens by three deuteriums, or the three <sup>35</sup>Cl by three <sup>37</sup>Cl); taken like this, the individual KIEs for these atoms was approximated by the cube root of the triply substituted KIE. Figure 4 depicts the KIE versus the inverse of the temperature, showing a flat curve below 10 K for all atoms (i.e. ground state tunneling), reaching 1.43 for H/D, 1.38 for <sup>10</sup>B/<sup>11</sup>B, and smaller values for the other atoms. Interestingly, nitrogen and hydrogen produce an inverse KIE at high temperatures due to their influence on the ZPE, but this effect is overcome by the mass effect on the tunneling rates at low temperatures. Note that due to the large H/D mass difference which produces enormous KIEs, the value for hydrogen cannot be compared to the other ratios.<sup>[81]</sup>

### 3. Conclusions

For the studied systems of acetonitrile-boron halides (MeCN–BX<sub>3</sub>, X=Cl, Br) and haloacetonitrile-boron chlorides (RCN–BCl<sub>3</sub>, R=CICH<sub>2</sub>, BrCH<sub>2</sub>), the adducts present a “weak form” of bond-stretch isomerism between a van der Waals interaction and a dative covalent bond. Computational analysis through the activation strain model, energy decomposition analysis, and natural bond analysis showed that these two minima in the potential energy surface occur due to an interplay between bond-distance dependent electrostatic and charge transfer

interactions working in opposition to the pyramidalization strain of the boron species.

Despite the appearance of these two theoretical minima, we proposed that the “long bond” configuration is probably impossible to detect experimentally even close to the absolute zero thanks to a tunneling mechanism that will swiftly turn it into the “short bond” structure. The flat Arrhenius curve below 10 K and the kinetic isotope effects analysis indicate that the rearrangement between these isomers is driven by boron atom tunneling. This prediction is consistent with previous experimental studies where the meta-stable, long bond structures were not detected in matrix-isolation setups. As such, we recommend considering the potential role of quantum tunneling when seeking elusive metastable species at cryogenic conditions; it might be that the nature of such compounds is more ephemeral than we suppose.

### Acknowledgements

This research was supported by the Israeli Science Foundation (grant no. 841/19) and the Netherlands Organization for Scientific Research (NWO). A.N. and N.T. acknowledges the Kreitman Graduate School of Advanced Studies for the Negev-Tsin and the mid-way Negev fellowships.

### Conflict of Interest

The authors declare no conflict of interest.

**Keywords:** heavy-atom tunneling · Lewis adduct · bond stretch isomerism · dative bond · kinetic isotope effect

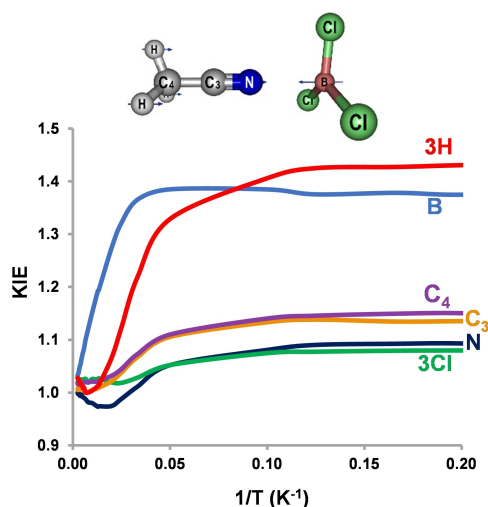


**Figure 4.** Kinetic isotope effects of MeCN–BCl<sub>3</sub> for <sup>10</sup>B/<sup>11</sup>B, <sup>14</sup>N/<sup>15</sup>N, <sup>35</sup>Cl/<sup>37</sup>Cl, <sup>12</sup>C/<sup>13</sup>C, and H/D substitutions, along with the activated complex showing the displacement vectors of the imaginary frequency.

- [1] W. D. Stohrer, R. Hoffmann, *J. Am. Chem. Soc.* **1972**, *94*, 779–786.
- [2] W. D. Stohrer, R. Hoffmann, *J. Am. Chem. Soc.* **1972**, *94*, 1661–1668.
- [3] A. V. Butcher, J. Chatt, *J. Chem. Soc. A* **1970**, 2652–2656.
- [4] K. Wieghardt, G. Backes-Dahmann, B. Nuber, J. Weiss, *Angew. Chem. Int. Ed. Engl.* **1985**, *24*, 777–778.
- [5] Y. Jean, A. Lledos, J. K. Burdett, R. Hoffmann, *J. Am. Chem. Soc.* **1988**, *110*, 4506–4516.
- [6] F. A. Cotton, M. P. Diebold, W. J. Roth, *Inorg. Chem.* **1987**, *26*, 2848–2852.
- [7] M.-M. Rohmer, M. Bénard, *Chem. Soc. Rev.* **2001**, *30*, 340–354.
- [8] Y. Jean, A. Lledos, J. K. Burdett, R. Hoffmann, *J. Chem. Soc. Chem. Commun.* **1988**, *0*, 140–142.
- [9] K. Yoon, G. Parkin, A. L. Rheingold, *J. Am. Chem. Soc.* **1992**, *114*, 2210–2218.
- [10] K. Yoon, G. Parkin, A. L. Rheingold, *J. Am. Chem. Soc.* **1991**, *113*, 1437–1438.
- [11] F. P. D. Nicola, M. Lanzi, F. Marchetti, G. Pampaloni, S. Zacchini, *Dalton Trans.* **2015**, *44*, 12653–12659.
- [12] J. Song, M. B. Hall, *Inorg. Chem.* **1991**, *30*, 4433–4437.
- [13] H. Shorafa, D. Mollenhauer, B. Paulus, K. Seppelt, *Angew. Chem. Int. Ed.* **2009**, *48*, 5845–5847; *Angew. Chem.* **2009**, *121*, 5959–5961.
- [14] A. Rodriguez, R. A. Olsen, N. Ghaderi, D. Scheschkewitz, F. S. Tham, L. J. Mueller, G. Bertrand, *Angew. Chem. Int. Ed.* **2004**, *116*, 4988–4991.
- [15] P. von R. Schleyer, A. F. Sax, J. Kalcher, R. Janoschek, *Angew. Chem. Int. Ed.* **1987**, *26*, 364–366; *Angew. Chem.* **1987**, *99*, 374–377.
- [16] J. A. Boatz, M. S. Gordon, *Organometallics* **1996**, *15*, 2118–2124.
- [17] U. Kölle, J. Kossakowski, N. Klaff, L. Wesemann, U. Englert, G. E. Herberich, *Angew. Chem. Int. Ed.* **1991**, *30*, 690–691; *Angew. Chem.* **1991**, *103*, 732–733.

- [18] J. E. McGrady, *Angew. Chem. Int. Ed.* **2000**, *39*, 3077–3079; *Angew. Chem.* **2000**, *112*, 3216–3219.
- [19] R. S. Mulliken, W. B. Person, *Molecular Complexes: A Lecture and Reprint Volume*. John Wiley & Sons, New York, **1969**.
- [20] R. Foster, *J. Phys. Chem.* **1980**, *84*, 2135–2141.
- [21] J. Yarwood, Ed., *Spectroscopy and Structure of Molecular Complexes*, Springer US, **1973**.
- [22] V. Jonas, G. Frenking, M. T. Reetz, *J. Am. Chem. Soc.* **1994**, *116*, 8741–8753.
- [23] G. Frenking, K. Wichmann, N. Fröhlich, C. Loschen, M. Lein, J. Frunzke, V. M. Rayón, *Coord. Chem. Rev.* **2003**, *238–239*, 55–82.
- [24] D. F. Shriver, B. Swanson, *Inorg. Chem.* **1971**, *10*, 1354–1365.
- [25] K. F. Purcell, R. S. Drago, *J. Am. Chem. Soc.* **1966**, *88*, 919–924.
- [26] K. R. Leopold, M. Canagaratna, J. A. Phillips, *Acc. Chem. Res.* **1997**, *30*, 57–64.
- [27] J. A. Phillips, *Theor. Chem. Acc.* **2016**, *136*, 16.
- [28] R. H. Crabtree, *Chem. Soc. Rev.* **2017**, *46*, 1720–1729.
- [29] J. P. Wrass, D. Sadowsky, K. M. Bloomgren, C. J. Cramer, J. A. Phillips, *Phys. Chem. Chem. Phys.* **2014**, *16*, 16480–16491.
- [30] J. A. Phillips, S. J. Danforth, N. J. Hora, J. R. Lanska, A. W. Waller, *J. Phys. Chem. A* **2017**, *121*, 9252–9261.
- [31] W. T. Borden, *WIREs Comput. Mol. Sci.* **2015**, *6*, 20–46.
- [32] J. Meisner, J. Kästner, *Angew. Chem. Int. Ed.* **2016**, *55*, 5400–5413; *Angew. Chem.* **2016**, *128*, 5488–5502.
- [33] C. Castro, W. L. Karney, *Angew. Chem. Int. Ed.* **2020**, *59*, 8355–8366; *Angew. Chem.* **2020**, *132*, 8431–8442.
- [34] A. Nandi, S. Kozuch, J. Kästner, *Chem. Phys. Lett.* **2020**, *754*, 137678.
- [35] P. R. Schreiner, *Trends Chem.* **2020**, *2*, 980–989.
- [36] P. R. Schreiner, *J. Am. Chem. Soc.* **2017**, *139*, 15276–15283.
- [37] M. J. Frisch, G. W. Trucks, H. B. Schlegel, G. E. Scuseria, M. A. Robb, J. R. Cheeseman, G. Scalmani, V. Barone, G. A. Petersson, H. Nakatsuji, X. Li, M. Caricato, A. V. Marenich, J. Bloino, B. G. Janesko, R. Gomperts, B. Mennucci, H. P. Hratchian, J. V. Ortiz, A. F. Izmaylov, J. L. Sonnenberg, D. Williams-Young, F. Ding, F. Lipparini, F. Egidi, J. Goings, B. Peng, A. Petrone, T. Henderson, D. Ranasinghe, V. G. Zakrzewski, J. Gao, N. Rega, G. Zheng, W. Liang, M. Hada, M. Ehara, K. Toyota, R. Fukuda, J. Hasegawa, M. Ishida, T. Nakajima, Y. Honda, O. Kitao, H. Nakai, T. Vreven, K. Throssell, J. A. Montgomery, Jr., J. E. Peralta, F. Ogliaro, M. J. Bearpark, J. J. Heyd, E. N. Brothers, K. N. Kudin, V. N. Staroverov, T. A. Keith, R. Kobayashi, J. Normand, K. Raghavachari, A. P. Rendell, J. C. Burant, S. S. Iyengar, J. Tomasi, M. Cossi, J. M. Millam, M. Klene, C. Adamo, R. Cammi, J. W. Ochterski, R. L. Martin, K. Morokuma, O. Farkas, J. B. Foresman, and D. J. Fox, Gaussian, Inc., Wallingford CT, 2016, n.d. M. J. Frisch, *Gaussian 16, Revision A.03, Gaussian, Inc., Wallingford, CT 2016*.
- [38] S. Kozuch, J. M. L. Martin, *J. Chem. Theory Comput.* **2013**, *9*, 1918–1931.
- [39] D. G. Truhlar, B. C. Garrett, *Annu. Rev. Phys. Chem.* **1984**, *35*, 159–189.
- [40] A. Fernandez-Ramos, B. A. Ellingson, B. C. Garrett, D. G. Truhlar, in *Reviews in Computational Chemistry*, Wiley-Blackwell, **2007**, pp. 125–232.
- [41] R. T. Skodje, D. G. Truhlar, B. C. Garrett, *J. Chem. Phys.* **1982**, *77*, 5955–5976.
- [42] J. G. Lauderdale, D. G. Truhlar, *Surf. Sci.* **1985**, *164*, 558–588.
- [43] Y.-Y. Chuang, J. C. Corchado, D. G. Truhlar, *J. Phys. Chem. A* **1999**, *103*, 1140–1149.
- [44] L. P. Viegas, A. J. C. Varandas, *J. Comput. Chem.* **2014**, *35*, 507–517.
- [45] L. P. Viegas, C. M. Nunes, R. Fausto, *Phys. Chem. Chem. Phys.* **2021**, *23*, 5797–5803.
- [46] A. Karton, P. R. Spackman, *J. Comput. Chem.* **2021**, *42*, 1590–1601.
- [47] J. Zheng, S. Zhang, B. J. Lynch, J. C. Corchado, Yao-Yuan, Chuang, P. L. Fast, W.-P. Hu, Y.-P. Liu, G. C. Lynch, K. A. Nguyen, C. F. Jackels, A. F. Ramos, B. A. Ellingson, V. S. Melissas, JordiVilà, I. Rossi, Elena. L. Coitiño, J. Pu, T. V. Albu, *POLYRATE, version 2016–2 A, University of Minnesota, Minneapolis, MN 2016*.
- [48] J. Zheng, S. Zhang, J. C. Corchado, Y. Y. Chuang, E. L. Coitino, B. A. Ellingson, D. G. Truhlar, *GAUSSRATE, version 2016, University of Minnesota, Minneapolis, MN, 2016*.
- [49] H. Amlani, A. Frenklah, S. Kozuch, in *Tunnelling in Molecules*, **2020**, pp. 61–87.
- [50] P. Vermeeren, S. C. C. van der Lubbe, C. Fonseca Guerra, F. M. Bickelhaupt, T. A. Hamlin, *Nat. Protoc.* **2020**, *15*, 649–667.
- [51] F. M. Bickelhaupt, K. N. Houk, *Angew. Chem. Int. Ed.* **2017**, *56*, 10070–10086; *Angew. Chem.* **2017**, *129*, 10204–10221.
- [52] L. P. Wolters, F. M. Bickelhaupt, *WIREs Comput. Mol. Sci.* **2015**, *5*, 324–343.
- [53] I. Fernández, F. M. Bickelhaupt, *Chem. Soc. Rev.* **2014**, *43*, 4953–4967.
- [54] W.-J. van Zeist, F. M. Bickelhaupt, *Org. Biomol. Chem.* **2010**, *8*, 3118–3127.
- [55] F. M. Bickelhaupt, *J. Comput. Chem.* **1999**, *20*, 114–128.
- [56] T. A. Hamlin, P. Vermeeren, C. Fonseca Guerra, F. M. Bickelhaupt, *Complementary Bonding Analysis*, (Eds.: S. Grabowsky), De Gruyter, Berlin, **2021**.
- [57] F. M. Bickelhaupt, E. J. Baerends, in *Reviews in Computational Chemistry*, John Wiley & Sons, Ltd, **2000**, pp. 1–86.
- [58] R. van Meer, O. V. Gritsenko, E. J. Baerends, *J. Chem. Theory Comput.* **2014**, *10*, 4432–4441.
- [59] E. van Lenthe, R. van Leeuwen, E. J. Baerends, J. G. Snijders, *Int. J. Quantum Chem.* **1996**, *57*, 281–293.
- [60] E. van Lenthe, E. J. Baerends, J. G. Snijders, *J. Chem. Phys.* **1994**, *101*, 9783–9792.
- [61] Y. Zhao, D. G. Truhlar, *Theor. Chem. Acc.* **2008**, *120*, 215–241.
- [62] E. V. Zeist, E. J. Baerends, *J. Comput. Chem.* **2003**, *24*, 1142–1156.
- [63] G. te Velde, F. M. Bickelhaupt, E. J. Baerends, C. Fonseca Guerra, S. J. A. van Gisbergen, J. G. Snijders, T. Ziegler, *J. Comput. Chem.* **2001**, *22*, 931–967.
- [64] C. Fonseca Guerra, J. G. Snijders, G. te Velde, E. J. Baerends, *Theor. Chem. Acc.* **1998**, *99*, 391–403.
- [65] ADF2019.305, SCM Theoretical Chemistry; Vrije Universiteit, Amsterdam, The Netherlands, www.scm.com.
- [66] W.-J. V. Zeist, C. Fonseca Guerra, F. M. Bickelhaupt, *J. Comput. Chem.* **2008**, *29*, 312–315.
- [67] X. Sun, T. M. Soini, J. Poater, T. A. Hamlin, F. M. Bickelhaupt, *J. Comput. Chem.* **2019**, *40*, 2227–2233.
- [68] PyFrag 2007–2020: X. Sun, T. Soini, L. P. Wolters, W.-J. van Zeist, C. Fonseca Guerra, T. A. Hamlin, F. M. Bickelhaupt, Vrije Universiteit Amsterdam, The Netherlands.
- [69] A. E. Reed, L. A. Curtiss, F. Weinhold, *Chem. Rev.* **1988**, *88*, 899–926.
- [70] A. J. Pounds, *J. Chem. Educ.* **2007**, *84*, 43.
- [71] D. J. Giesen, J. A. Phillips, *J. Phys. Chem. A* **2003**, *107*, 4009–4018.
- [72] J. A. Phillips, C. J. Cramer, *J. Phys. Chem. B* **2007**, *111*, 1408–1415.
- [73] E. V. Anslyn, D. A. Dougherty, *Modern Physical Organic Chemistry*, University Science, Sausalito, CA, **2005**.
- [74] D. Rodrigues Silva, L. de Azevedo Santos, M. P. Freitas, C. Fonseca Guerra, T. A. Hamlin, *Chem. Asian J.* **2020**, *15*, 4043–4054.
- [75] I. Alkorta, J. Elguero, J. E. Del Bene, O. Mó, M. Yáñez, *Chem. Eur. J.* **2010**, *16*, 11897–11905.
- [76] B. D. Rowsell, R. J. Gillespie, G. L. Heard, *Inorg. Chem.* **1999**, *38*, 4659–4662.
- [77] S. Kozuch, *Phys. Chem. Chem. Phys.* **2015**, *17*, 16688–16691.
- [78] S. Kozuch, *Org. Lett.* **2014**, *16*, 4102–4105.
- [79] A. Nandi, A. Sucher, A. Tyomkin, S. Kozuch, *Pure Appl. Chem.* **2020**, *92*, 39–47.
- [80] E. Solel, S. Kozuch, *J. Org. Chem.* **2018**, *83*, 10826–10834.
- [81] R. P. Bell, *The Tunneling Effect in Chemistry*, Chapman And Hall, London, **1980**.

Manuscript received: July 5, 2021  
Accepted manuscript online: July 10, 2021  
Version of record online: August 6, 2021